

# Spectroscopy of SN 1987A at 0.9–2.4 $\mu\text{m}$ : Days 1348–3158

A. Fassia<sup>1</sup>, W.P.S. Meikle<sup>1</sup> and J. Spyromilio<sup>2</sup>

<sup>1</sup>*Astrophysics Group, Blackett Laboratory, Imperial College, Prince Consort Rd, London SW7 2BZ, UK*

<sup>2</sup>*European Southern Observatory, Karl-Schwarzschild-Strasse 2, Garching, Germany*

28 October 2018

## ABSTRACT

We present near-infrared spectroscopic observations of SN 1987A covering the period 1358 to 3158 days post-explosion. This is the first time that IR spectra of a supernova have been obtained to such late epochs. The spectra comprise emission from both the ejecta and the bright, ring-shaped circumstellar medium (CSM). The most prominent CSM emission lines are recombination lines of H I and He I, and forbidden lines of [S III] and [Fe II]. The ejecta spectra include allowed lines of H I, He I and Na I and forbidden lines of [Si I], [Fe I], [Fe II], and possibly [S I]. The intensity ratios and widths of the H I ejecta lines are consistent with a low-temperature Case B recombination spectrum arising from non-thermal ionisation/excitation in an extended, adiabatically cooled H-envelope, as predicted by several authors. The slow decline of the ejecta forbidden lines, especially those of [Si I], indicates that pure non-thermal excitation was taking place, driven increasingly by the decay of <sup>44</sup>Ti. The ejecta iron exhibits particularly high velocities (4000–4500 km/s), supporting scenarios where fast radioactive nickel is created and ejected just after the core-bounce. In addition, the ejecta lines continue to exhibit blueshifts with values  $\sim -200$  km/s to  $-800$  km/s to at least day 2000. These blueshifts, which first appeared around day 600, probably indicate that very dense concentrations of dust persist in the ejecta, although an alternative explanation of asymmetry in the excitation conditions is not ruled out.

**Key words:** Supernovae: individual (SN 1987A), dust infrared, circumstellar matter

## 1 INTRODUCTION

The exceptionally close proximity of the type IIpec supernova SN 1987A in the Large Magellanic Cloud has provided a unique opportunity to observe a core-collapse supernova with all the resources of modern observational astronomy and over a very long period of time. Near-infrared (near-IR) spectroscopy has played a vital role in the determination of the physical conditions in the debris and the investigation of the element synthesis, providing a valuable complement to optical spectra. In particular, in the nebular phase (when the lines are mostly optically thin) the line profiles produced in the high velocity, homologous expansion have enabled us to examine the ejecta abundances and their *spatial* distribution. During the first few years, all the major southern observatories obtained near-IR spectra of SN 1987A. Observations at the Anglo-Australian Telescope (AAT) covering the first 3 years post-explosion were described in Meikle et al. (1989, 1993) (hereinafter Papers I, II).

a further 8 epochs from 1990 November 2 (day 1348 = 3.7 years) to 1995 October 17 (day 3158 = 8.6 years). Epochs are with respect to the explosion date 1987 February 23. Our day 1348 spectrum was the last observation of SN 1987A obtained with the near-IR spectrometer FIGS (Bailey et al. 1988. Also see Papers I & II). All the subsequent spectra were obtained with the more sensitive spectrograph, IRIS (Allen et al. 1993), which allowed the acquisition of high resolution near-IR spectra to a later phase than was achieved at any other observatory. Preliminary reports of these data have been given in Fassia (1999) and Meikle (2001). The only other post-3 year IR spectra reported are those of Bautista et al. (1995) which reached day 1445, but at a lower resolution than those described here. In a future paper (Fassia et al., in preparation) we shall present *HK*-band spectra of SN 1987A taken with the MPE imaging spectrograph, 3D (Weitzel et al. 1996), at the AAT on 1997 Dec 16 (day 3949 = 10.8 years) and 1998 Dec 1 (day 4299 = 11.8 years). We also note that the earliest Hubble Space Telescope (HST) NICMOS spectrum of SN 1987A was taken on 1998 June 15 (day 4130 = 11.3 years), but has not yet been published.

In this paper we describe spectra obtained at the AAT for

## 2 OBSERVATIONS

The observations are summarised in Table 1. Some of the data presented here were obtained in runs of several days. In the text and diagrams these runs will usually be identified by the epoch of the first day of each. For further details of the FIGS spectrometer, used to obtain the day 1348 spectrum, see Bailey et al. (1988) and Papers I & II. The IRIS spectrograph was based on a  $128 \times 128$  pixel HgCdTe array. All the IRIS observations were taken at  $f/36$ , yielding a plate scale of 0.79 arcsec/pixel. Spectra were acquired in the echelle mode for epochs 1469–2112 days and in the  $H$ -grism mode for the subsequent epochs. In the echelle mode, 4 orders of cross-dispersed spectra were provided, covering 0.9–1.5  $\mu\text{m}$  ( $IJ$  band) and 1.4–2.4  $\mu\text{m}$  ( $HK$  band). The slit was usually oriented at a P.A. of 90 deg. *i.e.* east-west. The slit length was 13 arcsec (16 pixels) while in the dispersion direction, 2 pixels corresponded to a spectral resolution of about 375 ( $\lambda/\Delta\lambda$ ) (equivalent to  $\sim 800$  km/s). However, the actual resolution was generally poorer than this (see below). To enable sky-subtraction, the telescope was nodded along the slit by 5–8 arcsec (6–10 pixels). To improve the flux measurement precision of both the ejecta and the bright ring, the slit width for the  $IJ$  observations was set at 5.8 arcsec. Similarly, the 1348 d FIGS spectrum was obtained with a 5.9 arcsec aperture. Thus, the resolution of the (point-source) ejecta spectra was effectively determined by the seeing. For the CSM spectra, the finite extent of the bright ring ( $1.66 \times 1.21$  arcsec, Plait et al. 1995) would have produced a slightly lower resolution. The  $IJ$  echelle resolutions listed in Table 1, column 4, were obtained directly from the FWHM of the He I 1.083  $\mu\text{m}$  line. They were typically 200–400 ( $\lambda/\Delta\lambda$ ). As already mentioned, the resolution of the ejecta spectra was probably slightly higher. For the  $HK$  observations, we were unable to use the 5.8 arcsec slit since it produced severe degradation of the S/N. We therefore used a slit width of 1.4 arcsec in this band. The  $HK$  resolution was obtained from the FWHM of the He I 2.058  $\mu\text{m}$  CSM line. Owing to the declining flux, after day 2112, spectra were taken using the lower resolution  $H$ -grism mode. This covered 1.2–2.1  $\mu\text{m}$  in a single order. The slit was usually oriented at a P.A. of 135 deg. in order to maximise the spatial separation of the spectra of the supernova and Stars 2 and 3 (see below). The slit length was 24 arcsec (30 pixels), while in the dispersion direction a 1.6 arcsec (2 pixel) wide slit was used, yielding a spectral resolution of 120 ( $\lambda/\Delta\lambda$ ) (equivalent to  $\sim 2,500$  km/s). The nod throw was 10–15 arcsec.

The day 1348 FIGS spectrum was reduced using FIGARO (Shortridge 1995). Final fluxing was by comparison with contemporary broad-band photometry obtained with the AAT IR photometer IRPS (*cf.* procedure described in Paper II), using the A7 dwarf BS 2015 as the local standard. However, by this epoch, the narrow He I 1.083  $\mu\text{m}$  line from the bright ring had an intensity of about 20% of the flux within the  $J$ -photometry wavelength window. Moreover it lay right at the blue edge of the  $J$ -band filter, making it difficult to judge the effect of the bright ring on the  $J$ -magnitude. (The spatial coverage of IRPS included the ring). Therefore, taking into account other uncertainties, we judge the uncertainty in the fluxing to be of order  $\pm 25\%$ . The wavelength

scale was calibrated using the narrow He I 1.083  $\mu\text{m}$  and Pa $\beta$  lines, adopting a redshift of +289 km/s (Crotts & Heathcote 1991).

The IRIS data were also reduced using FIGARO. After bias-subtraction and flat-field correction the image-pair obtained at the two nod positions were subtracted to remove sky line emission. For the echelle-mode data, different echelle orders were then traced and corrected for echelle distortion. The positive and negative spectra were extracted from the resulting frames using simple extraction. We extracted over 4–6 pixel rows (3.2–4.8 arcsec), depending on the seeing. This is discussed further below. Cosmic rays and residual sky-lines were identified and removed by comparing repeat observations of spectra obtained at different times during the night. Wavelength calibration was by means of argon and xenon arc lamps and the night-sky emission lines present in the supernova spectra. The wavelength uncertainty in the echelle spectra ranges from  $\pm 0.0014$   $\mu\text{m}$  in the  $IJ$ -band spectra to  $\pm 0.0025$   $\mu\text{m}$  in the  $HK$ -band spectra. The wavelength uncertainty in the grism spectra is  $\pm 0.009$   $\mu\text{m}$ . To correct for the atmospheric and instrumental transmission functions and to flux-calibrate the spectra, we used the G dwarf spectrophotometric standard BS 1294 (Allen & Cragg 1983). The adopted magnitudes were  $J=+5.20$ ,  $H=+4.90$ ,  $K=+4.84$ . (For the grism spectrum on day 3158, we used the A4 giant HD 19904, adopting  $H=+6.66$ ). The spectral orders of the echelle spectra were then merged to form single spectra. The final fluxing of the spectra is now described.

Accurate flux calibration of the spectra was difficult and became increasingly so with time. This was due to the combined effects of the declining SN flux, variable seeing, variable atmospheric transmission for both supernova and standard (the airmass was inevitably quite high *viz.* 1.4–1.8), pointing errors of up to  $\sim 2$  arcsec and, for the echelle spectra, the small number of detector pixels (16) along the slit in a given order. Flux measurement under poor seeing conditions was a particular problem for the narrow slit spectra due to the greater (but uncertain) vignetting effects. However, the most difficult problem of all in the flux calibration procedure was contamination by light from the nearby Star 3, and even from the slightly more distant Star 2. To make matters worse, Star 3 is a variable Be star. Around day 1500 the IR fluxes from Stars 2 and 3 were about  $\times 1.4$  and  $\times 0.85$ , respectively, of the SN flux, rising to about  $\times 4$  and  $\times 1.5$  by day 2112 (Walborn et al. 1993, Suntzeff private communication. See also Turner et al. (1996)). Star 2 lies at 2.9 arcsec from the SN, at PA =  $311^\circ$  while Star 3 lies at 1.6 arcsec distance at PA =  $117^\circ$  (Walker & Suntzeff 1990). Thus, for the typical E-W slit orientation used for echelle spectra, the distances of Stars 2 and 3 from SN 1987A, along the slit, were only  $\sim 2.2$  and  $\sim 1.5$  arcsec respectively. (We note that even at our latest epoch, the intrinsic diameter of the ejecta source was probably less than 0.1 arcsec (Jakobsen et al. 1994), and so was effectively a point source whose observed extent was entirely determined by the seeing.) Thus, under typical seeing conditions, the Star 3 spectrum was spatially blended with the spectra of both the ejecta and bright ring of SN 1987A, while under poor seeing conditions even Star 2 could significantly contaminate the SN light. The grism spectra of days 2952 and 3158 were taken with a

slit PA of  $135^\circ$  yielding slightly larger displacements of the stars along the slit. However, the much reduced flux from the supernova by these epochs meant that contamination of the SN light by the nearby stars was still a problem. The contamination from both stars took the form of a continuum of uncertain flux, together with possible narrow H and He emission lines from Star 3 (Walborn et al. 1993).

Assessment and removal of the contaminating light presented a difficult challenge. Even with the wide slit, variations in the seeing conditions and/or telescope pointing precision could make the degree of contamination within the slit difficult to estimate. (A further complicating factor was that Star 3 itself could vary by up to a magnitude over a period of 800 days. However, the IR light curves of the star provided by (Walborn et al. 1993) meant that this variation could, in principle, be taken into account.) As already described, we extracted the spectra from 4–6 pixel rows (3.2–4.8 arcsec). Thus all the extracted spectra contained contamination from Star 3 and sometimes Star 2.

We first consider the removal of the continuum contamination from the ejecta spectra. We investigated several methods using ground-based observations. However, internal consistency in the results eluded us, probably due to uncertainties in the variable factors already described. Therefore, we decided that the best solution was to make use of the high spatial resolution optical spectra provided by the HST. To determine the extent of the continuum contamination, we inspected the relatively uncontaminated optical HST spectra of the SN 1987A ejecta obtained on days 1862, 2210 (Wang et al. 1996) and 2875 (Chugai et al. 1997 (C97)). The red end (6000–8000 Å) of these spectra exhibits a weak, roughly flat continuum of  $1 - 2 \times 10^{-17} \text{ erg sec}^{-1} \text{ \AA}^{-1}$ . C97 and DeKool, Li & McCray (1998) (dKLM98) suggest that this is actually a quasi-continuum produced by the down-conversion of UV photons following absorption/emission by metals. We therefore assumed that the ejecta continuum in the near-IR bands should also be roughly flat. However, in the reduced IR spectra (before correction for stellar contamination), the continuum was observed to rise towards shorter wavelengths and so we attributed the rising portion to contamination from Stars 2 & 3. To remove the contamination, we first modelled the shape of the stellar continuum by fitting a blackbody of the appropriate temperature to the Star 3 infrared photometry of Walborn et al. (1993). Since Stars 2 & 3 are of a similar stellar type (B2) the model continuum was used to represent the combined effects of contamination from both stars. However, Star 3 was the dominant or even sole contaminator in all cases. We then scaled the model continuum and subtracted it from the reduced spectrum to try to produce a flat continuum. For most of the wavelength range covered, it was found that roughly flat continua could indeed be formed in this way. However, within the  $\sim 1.4 \mu\text{m}$ – $\sim 1.7 \mu\text{m}$  range a relatively abrupt decline, or “step” in the continuum persisted. We believe this step to be due to a real physical decline in the quasi-continuum of the ejecta, and is not due to the fact that the *IJ*, *HK* spectra were taken at different times and with different instrument settings. Our reasons are, firstly, the *IJ* spectra covered wavelengths up to  $1.5 \mu\text{m}$  and the beginning of the “step” is clearly present in these data alone. Secondly, the step can be seen in the

spectra taken at the AAT (Paper II) and at CTIO (Elias et al. 1991) at  $\sim 1000$  days, and in the day 1445 spectrum of Bautista et al. (1995).

To finally flux-calibrate the de-contaminated spectra we proceeded as follows. First we edited out the narrow lines, producing observed “pure-ejecta” spectra,  $S_{obs}(\lambda)$ . For the low-resolution grism spectra, this could only be done very approximately. However, the CSM line contribution to the flux in the wavelength region covered by the grism (1.2–2.1  $\mu\text{m}$ ) was probably small. This can be deduced by considering the CSM line fluxes (Table 3) at earlier epochs (days 1469–2112) when these lines were more clearly resolved. Comparison with contemporary pure-ejecta *JHK* band magnitudes obtained at CTIO (Suntzeff private communication) or with the empirical spectral model matches (Figs. 3–5) (see below) indicates that the CSM contribution was probably less than 20% of the total during this earlier phase, and showed little sign of increasing with time. We believe it is highly unlikely that a sudden rapid increase in the CSM contribution occurred by day  $\sim 3000$ .

We then scaled the individual *JHK* regions of the spectra to match the contemporary CTIO photometry. To find the scaling factors, we determined the true ejecta spectrum,  $S(\lambda)$ , using the relation

$$mag = -2.5 \log \int S(\lambda)T(\lambda)d\lambda + ZP, \quad (1)$$

where *mag* is the ejecta magnitude provided by Suntzeff, and  $T(\lambda)$  is the filter transmission function. *ZP* is the magnitude zero point given by  $ZP = 2.5 \log \int S_{Vega}(\lambda)T(\lambda)d\lambda$  where  $S_{Vega}(\lambda)$  is the flux of Vega derived from the Kurucz stellar atmosphere models (Kurucz 1993) using  $T_{eff} = 9,400 \text{ K}$  and  $\log g = 3.9$ . Adopting 0.0 as the *JHK* magnitude of Vega (Elias et al. 1982),  $S(\lambda)$  was determined for each band and epoch. The scaling factor,  $\phi$ , was then obtained from  $S(\lambda) = \phi \times S_{obs}(\lambda)$ .

To check the flux calibration procedure described above, we carried out the following test. The day 1734 *IJ* spectra were acquired under photometric conditions with good seeing, in a wide (5.8 arcsec) slit. Therefore it was reasonable to assume that the whole of the SN 1987A light and an uncertain amount of the Star 3 light were blended within the slit, and that the flux calibration via the spectrophotometric standard was reliable. We then edited out all the circumstellar lines from the reduced, standard-fluxed spectrum, yielding an unvignetted ejecta spectrum, but still blended an unknown (vignetted) fraction of the Star 3 continuum. We then scaled and subtracted a blackbody representation of Star 3, with the scaling adjusted so that, when multiplied by the CTIO filter function, the resulting SN 1987A ejecta spectrum matched the CTIO photometry. We found that the flux of the ejecta spectrum produced in this way differed from that obtained by the “flat-continuum” procedure by less than 5%. We concluded that the “flat-continuum” procedure was reliable, and so we applied the method to all the spectra. The factors by which the continuum-flattened spectra had to be scaled to match the photometry ranged from  $\times 0.3$  to  $\times 2.3$ , indicating the severity of the effects discussed above. Including uncertainties in the Star 3 subtraction, we

estimate the final absolute fluxing of the ejecta spectra to be accurate to better than  $\pm 40\%$ . The final spectra are shown in Figures 1–7.

We now turn briefly to the final fluxing of the CSM lines. We first consider the CSM spectra obtained in the higher resolution echelle mode. While uncertainties in the continuum was not a problem here, it was important to consider the effect of the extent of the ring ( $\sim 1.2$  arcsec in the dispersion direction). The echelle *IJ* spectra were obtained with a wide slit (5.8 arcsec). In addition, all spectra were extracted from a region of  $>3.2$  arcsec. It is likely, therefore, that any vignetting of the CSM flux was small. Possible narrow line contamination from the Be Star 3 was checked by inspection of unpublished NICMOS observations of this star taken on day 4130 (P. Challis & P. Garnavich, private communication). This showed that the contribution to the narrow He I 1.083  $\mu\text{m}$  line was less than 12%. We concluded that narrow line contamination was negligible. Thus, the errors in the *IJ* CSM line fluxes would be mostly of the same origin as those present in the post-flattened ejecta spectra (*e.g.* variable extinction). Consequently we corrected the *IJ* CSM line fluxes using the same scaling factors,  $\phi$ , as for the ejecta spectra. We judge the precision in the final *IJ* CSM spectra to be better than  $\pm 40\%$ . Owing to S/N problems (see above), the echelle *HK* spectra were obtained with a narrow slit (1.4 arcsec). Together with the effect of the typical 1.0–1.5 arcsec seeing, and pointing errors, this meant that quite significant vignetting of the CSM light probably occurred in the *HK* observations. We judge that as much as half the CSM light could have been “lost” in this way. Thus, while we also applied the  $\phi$  scaling factor to the *HK* CSM spectra, the effects of vignetting means that the *HK* CSM fluxes are very uncertain. For the last two epochs (days 2952 and 3158), not only was a narrow (1.6 arcsec) slit used, but the low resolution of the grism produced strong blending of the CSM and ejecta spectra. Consequently, no attempt has been made to extract CSM line fluxes for these last two epochs.

### 3 OVERVIEW OF THE SPECTRA

The spectra (Figs. 1–7) comprise broad resolved emission lines from the ejecta and narrow unresolved emission lines from the circumstellar ring, superimposed on a continuum. The continuum is roughly flat within most wavelength bands, but fades over the range 1.4–1.7  $\mu\text{m}$  by a factor of  $\sim 10$  on day 1533, and  $\sim 2$ –4 on days 1734, 1822 and 2122. As already indicated, we attribute the continuum to a blend of weak lines produced by the down-conversion of UV photons following absorption/emission by metals.

#### 3.1 Line identification and measurement

While it was straightforward to identify and measure the strongest or most isolated lines (*e.g.* the He I 1.083  $\mu\text{m}$  CSM line), most of the features comprised blends of lines from the ejecta and CSM and/or from different species. Therefore, in order to identify and measure the component lines, we proceeded as follows. Preliminary ejecta line identification was performed by selecting plausible candidate species from

the line identifications of Paper II and from the theoretical predictions of dKLM98 and Kozma & Fransson (1998a,b) (KF98a,b). Likewise, we used the work of Lundqvist & Sonneborn (2001) to provide suggestions for the CSM line identifications. Then, in order to confirm the line identifications and to measure the intensities, widths and wavelength shifts, we matched an empirical spectral model to the data. In this model, the continuum was represented by applying a smoothed spline fit to regions of the observed spectra which were clear of discrete emission features. Emission features were then superimposed on this continuum. These were selected using the aforementioned identification sources. Their profiles were represented using Gaussian profiles with the peak value as one of the free parameters.

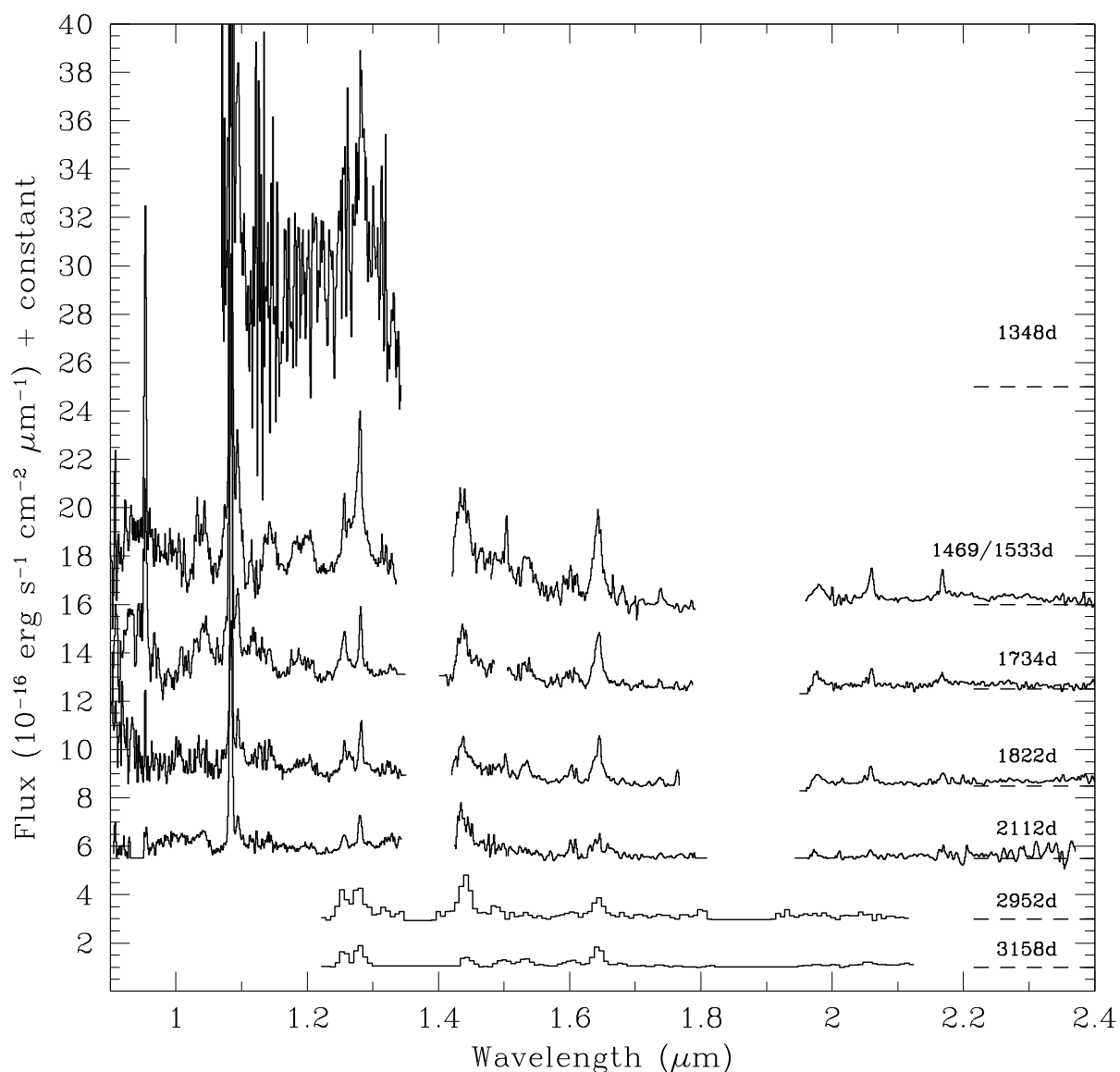
For the CSM lines, we assumed that the lines were redshifted by +289 km/s (Heathcote et al. 1991), and that their widths were defined by the prevailing spectral resolution. This resolution was measured from the strong He I 1.083  $\mu\text{m}$  CSM line for the *IJ* spectra, and the He I 2.058  $\mu\text{m}$  CSM line for the *HK* spectra (*cf.* Section 2). Within the [Fe II] multiplets (see below), the relative line intensities were derived by assuming that the population distribution within the upper term was determined by the Boltzmann distribution at 3000 K. While the CSM temperature was probably somewhat higher than this, it would have a negligible effect on the distribution within the small energy range of a term. For the [S III] CSM lines, direct measurement of the line intensities was judged to be more reliable than use of the model matches.

The empirical model ejecta line intensities, wavelength positions and widths were all allowed to vary under certain constraints. For a particular species (*e.g.* [Fe II]), individual linewidths and wavelength shifts were always set to be the same in velocity space. For the [Si I] and [S I] multiplets (see below), the components of each multiplet had the same upper level and so the intensity ratios of a given multiplet were found simply from the A-values and statistical weights alone. Given the uncertainty in the excitation conditions, determination of some of the intensity ratios within the [Fe I] and [Fe II] multiplets was less straightforward since some lines arose from different upper levels. In practice, to estimate the intensities of the other components we simply used the same multiplet ratios as for the CSM, adopting  $T=3000$  K. While this may have produced inappropriate relative intensities for some lines, it is likely that most of the weaker lines made only a minor contribution to the spectrum. We also note that for the most significant line ratio *viz.*  $I_{1.257\mu\text{m}}/I_{1.644\mu\text{m}}$ , the components (which are actually members of different multiplets) arose from the same upper level, and so could be estimated from the A-values and statistical weights alone. Matching was guided primarily by the absolute intensity of the dominant component in a given multiplet. For each observed spectrum, the spectral model was varied until a visually satisfactory match to the observed spectrum was achieved.

The model matches for epochs 1469 to 2112 are shown in Figures 2–5. Also shown (dotted lines) are the individual lines that make up each blend. It can be seen that some of the spectral features comprise quite complicated blends of

**Table 1.** Log of optical spectroscopy of SN 1987A

Date	Epoch (days)	Spectral Range ( $\text{\AA}$ )	Spectral Resn. ( $\lambda/\Delta\lambda$ )	Slit Width (arcsec)	Seeing (arcsec)
02 Nov 1990	1348	10690–13400	220	5.9	>1.5
03 Mar 1991	1469	8955–15120	385	5.8	1.0–3.0
06 May 1991	1533	14320–24450	350	1.4	$\sim$ 1.0
23 Nov 1991	1734	14550–24670	350	1.4	>1.0
24 Nov 1991	1735	9035–15110	270	5.8	$\sim$ 1.0
19 Feb 1992	1822	14720–24500	350	1.4	$\sim$ 1.5
20 Feb 1992	1823	9005–15050	270	5.8	1.0–3.0
05 Dec 1992	2112	9048–14326	185	5.8	$\sim$ 1.0
05 Dec 1992	2112	14690–24320	350	1.4	$\sim$ 1.0
25 Mar 1995	2952	12250–21134	120	1.6	1.3–2.5
17 Oct 1995	3158	12250–21110	120	1.6	$\sim$ 1.2

**Figure 1.** *IJHK* band spectra of SN 1987A obtained with the IRIS spectrograph at the Anglo-Australian Telescope. For clarity the spectra have been displaced vertically. Zero flux for each spectrum is shown by the horizontal dashed lines on the right hand side.

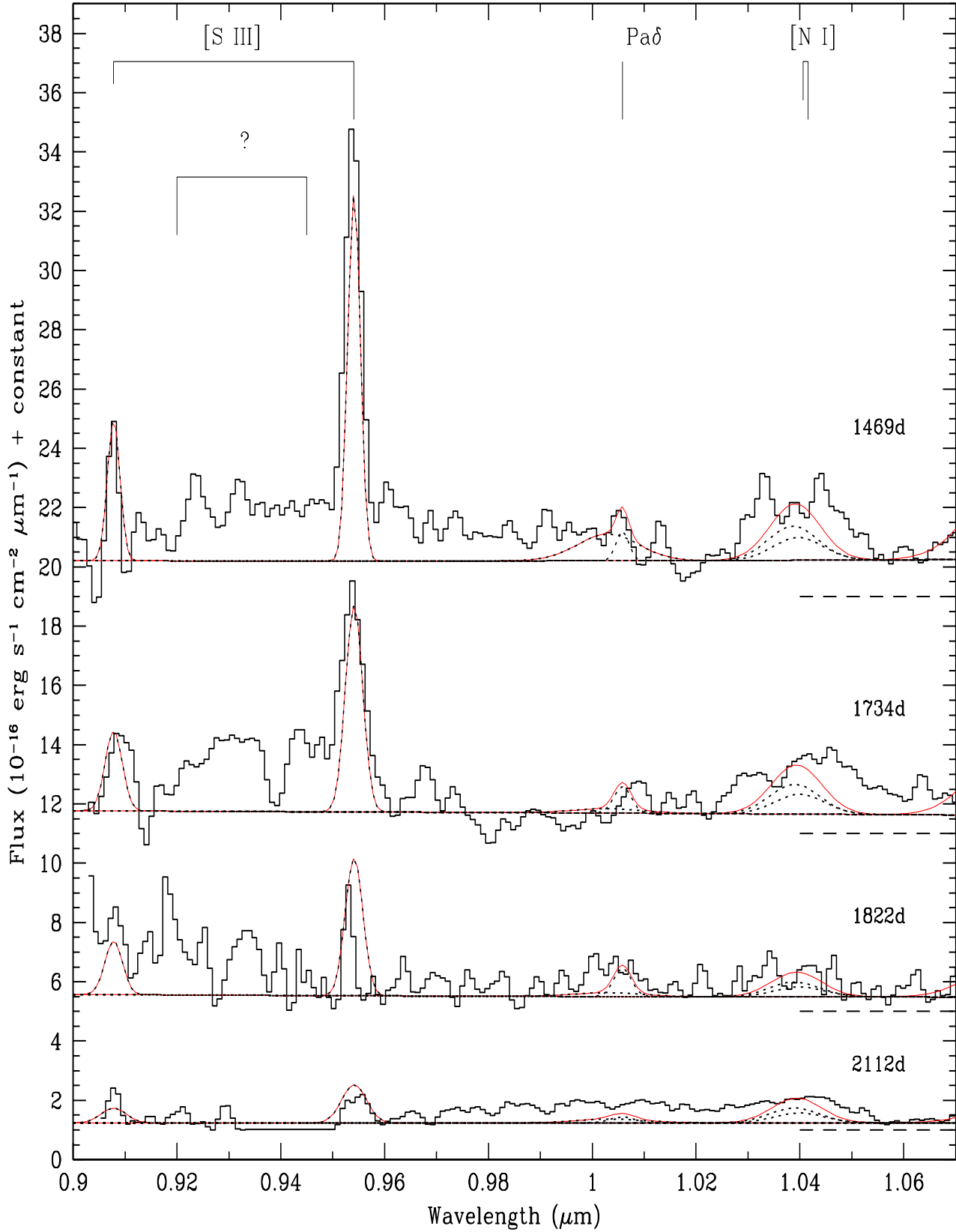


**Figure 2.** *I* band spectra (thick solid lines) of SN 1987A obtained with the IRIS spectrograph in echelle mode, at the Anglo-Australian Telescope. For clarity the spectra have been displaced vertically. Zero flux for each spectrum is shown by the horizontal dashed lines on the right hand side. The fluxes of the ejecta and *IJ*-band CSM spectra are estimated to be accurate to better than  $\pm 40\%$ . The thin solid lines show the empirical spectral model (see text). The individual line components are shown as dotted lines. Line identifications are given by the vertical markers at the top, placed at the rest wavelength for the SN 1987A centre-of-mass. Within a multiplet, the lengths of the markers are proportional to the component intensities (see text).

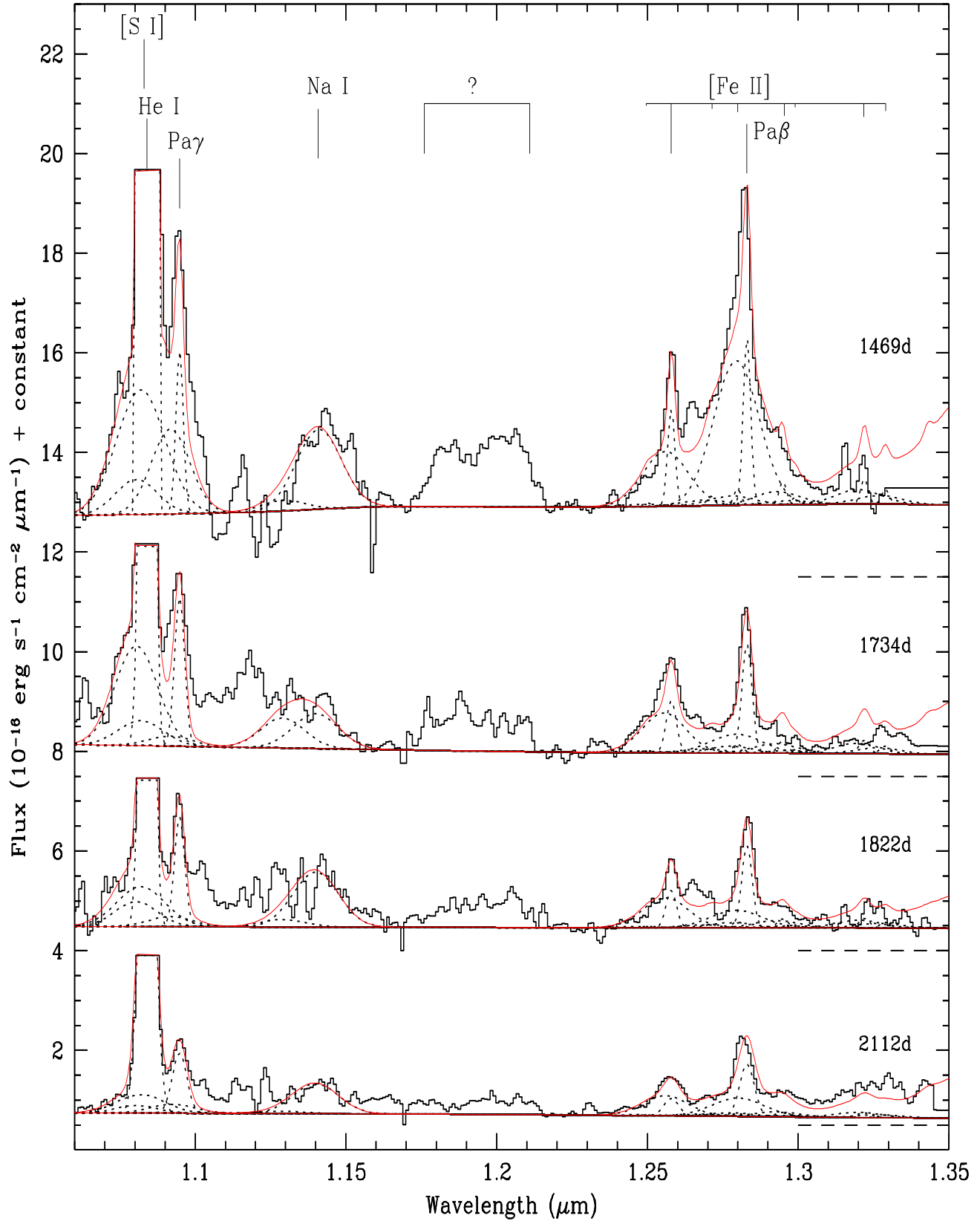


Figure 3. As Fig. 2, but for the *J* window. The strong He I 1.083  $\mu\text{m}$  CSM line has been truncated.

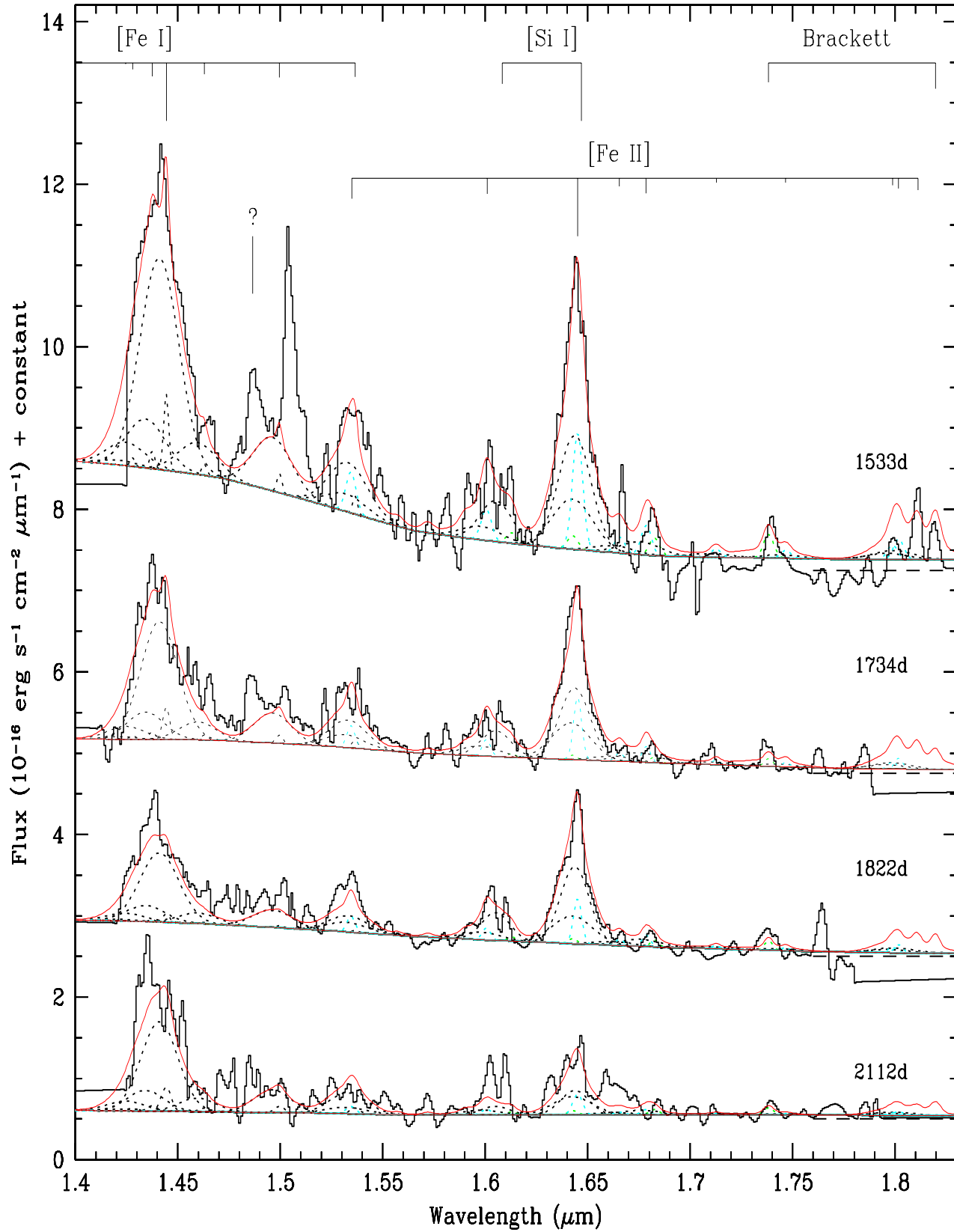


Figure 4. As Fig. 2, but for the *H* window. Fluxing of the *HK* CSM lines is only approximate (see text).



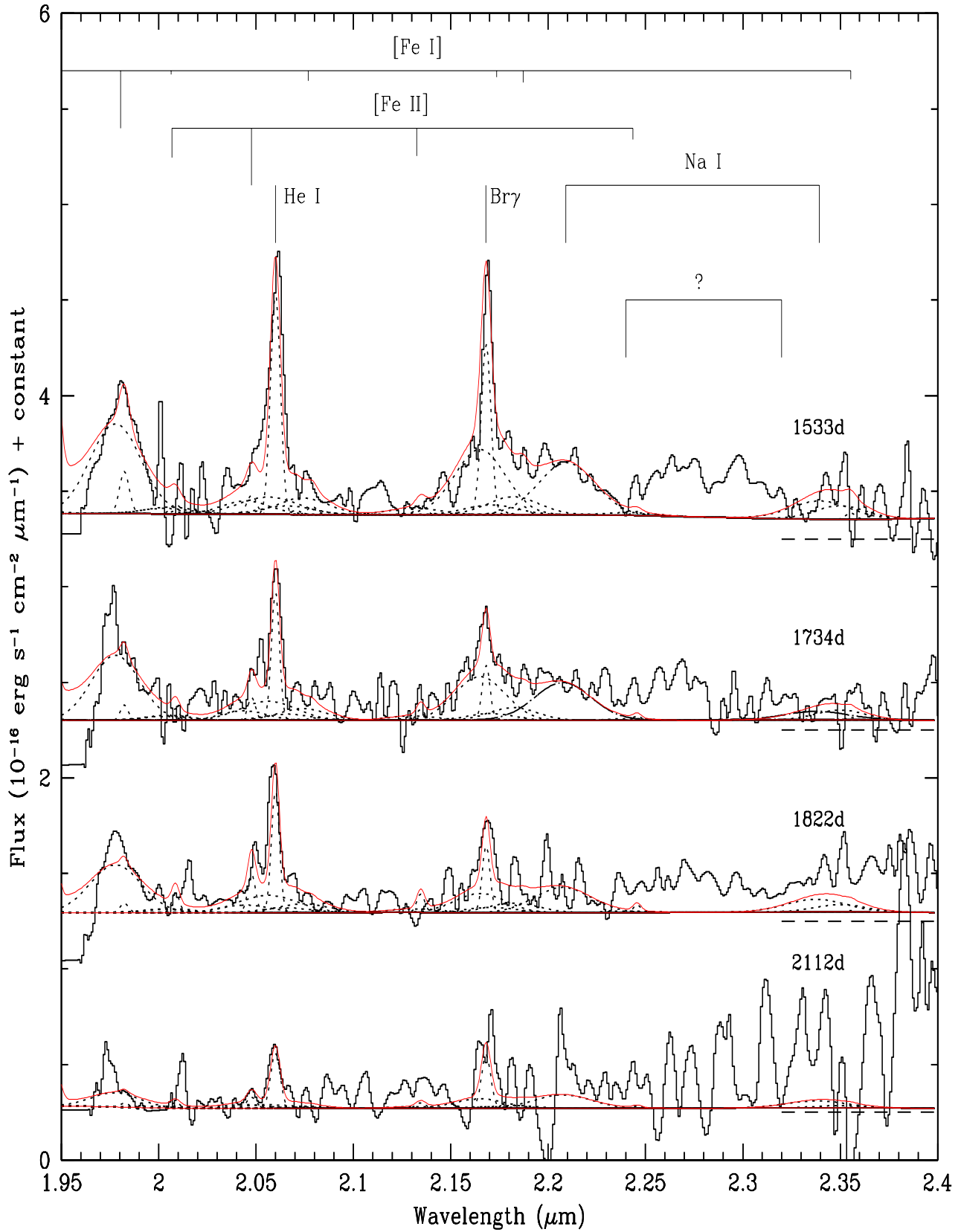
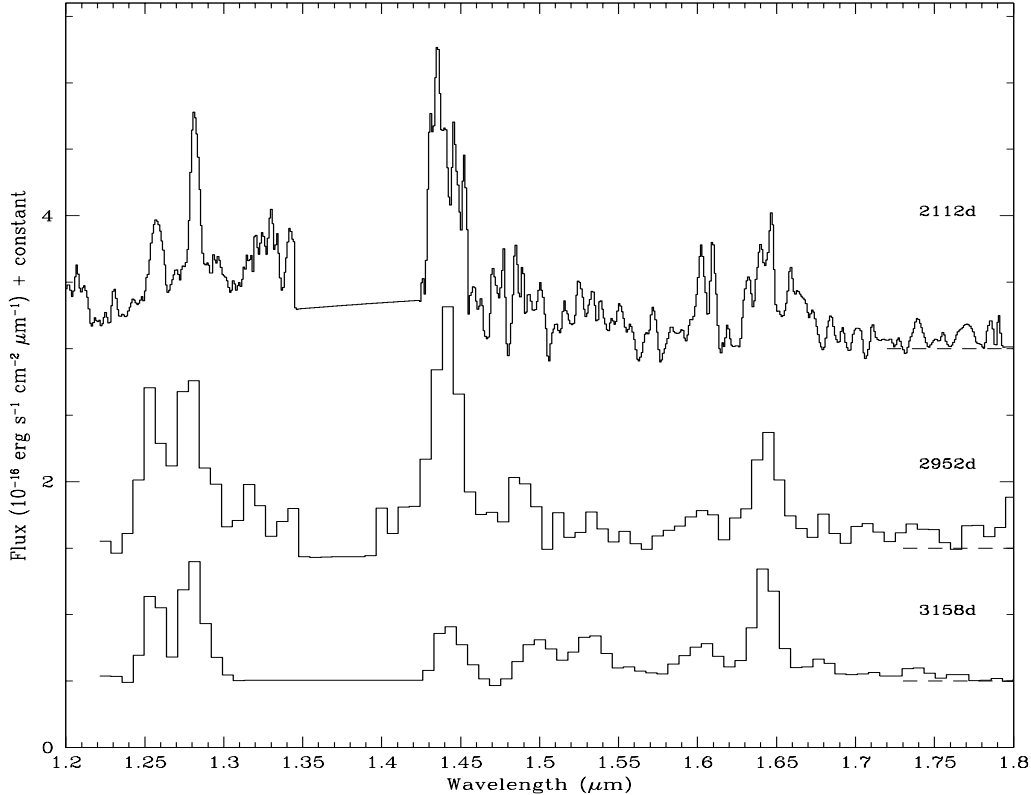


Figure 5. As Fig. 2, but for the  $K$  window. Fluxing of the  $HK$  CSM lines is only approximate (see text).



**Figure 6.** IRIS grism-mode spectra of SN 1987A obtained on days 2952 and 3158. Also shown is the last IRIS echelle spectrum (day 2112). For clarity the spectra have been displaced vertically. Zero flux for each spectrum is shown by the horizontal dashed lines on the right hand side.

ejecta and CSM lines. Details of the line parameters for the ejecta and CSM are given in Tables 2 and 3 respectively. In Table 2, Column 3 gives the displacement (in velocity space) of the line peak with respect to the wavelength of the identified line in the SN 1987A rest frame (redshift = +289 km/s). Column 4 gives the linewidths (FWHM), again in terms of equivalent velocity. The precision in the absolute intensities of the well-matched lines approaches that of the spectral fluxing precision (Section 2), with even higher accuracy for relative intensities within a single-band spectrum. However, in many cases the matching is more approximate with consequently poorer line intensity accuracy. This tends to be an increasing problem at later epochs. To assess the precision of a line intensity given in Table 1 or 2, the reader is advised to examine the quality of the model matches in the spectral plots (Figs. 2–5). Model matches were carried out only up to day 2112. The spectra for days 2952 and 3158 were judged to be of too low resolution and S/N to provide useful constraints on the model parameters. We therefore simply present these spectra, in Figure 6, compared with the final echelle spectrum taken on day 2112.

### 3.2 The ejecta lines

For the epochs covered by the echelle spectra (days 1469–2112), the most prominent ejecta emission features included H I ( $\text{Pa}\beta$ ,  $\text{Pa}\gamma$ ,  $\text{Br}\gamma$ ), He I 1.08, 2.06  $\mu\text{m}$ , Na I 1.14, 2.21, 2.34  $\mu\text{m}$ , [Si I] 1.61, 1.65  $\mu\text{m}$ , [Fe I] 1.44, 1.98  $\mu\text{m}$  and [Fe II] 1.26, 1.64, 2.05  $\mu\text{m}$ . [S I] 1.08, 1.13  $\mu\text{m}$  may also be present,

but strong blending with other lines renders this identification less positive. There were also regions of emission for which we were unable to find plausible identifications. These were at 0.92–0.95, 1.03–1.05, 1.17–1.21 and 2.24–2.32  $\mu\text{m}$ . The 1.03–1.05  $\mu\text{m}$  feature may be caused partly by [N I] 1.04  $\mu\text{m}$ . However, the width and shape of the feature indicates that there must be contributions from other species. The 1.17–1.21  $\mu\text{m}$  feature is particularly interesting in that it has persisted from as early as day 112 (Paper I). In Papers I and II we attributed this feature to a blend of allowed lines of Mg I, Si I and K I. However, its relatively unchanging shape between days 112 and 1822 prompts us to question if it really is a blend of different species. We also note that the 2.24–2.32  $\mu\text{m}$  emission lies in the same wavelength region as an unidentified feature discussed in Paper II.

### 3.3 The CSM lines

The principal CSM features were due to H I ( $\text{Pa}\beta$ ,  $\text{Pa}\gamma$ ,  $\text{Br}\gamma$ ), He I 1.08, 2.06  $\mu\text{m}$ , [S III] 0.91, 0.95  $\mu\text{m}$  and [Fe II] 1.26, 1.646, 2.05  $\mu\text{m}$ . Of particular note is the very strong He I 1.083  $\mu\text{m}$  line which contributes  $\sim 20\%$  of the total (ejecta+CSM)  $IJ$  band flux on day 1469 and 13–11% on days 1734–2112 (Figure 7). We believe that [S III] 0.907, 0.953  $\mu\text{m}$  lines have never before been reported in a supernova spectrum. Their presence in the spectra of days 1469 and 1734 is particularly convincing. The lines are less apparent in the day 1822 and 2112 spectra due to the fading flux and the poorer observing conditions at these epochs. We

**Table 2.** Major ejecta emission features observed on days 1469 to 2112

Epoch (days)	$\lambda_{peak}$ ( $\mu\text{m}$ )	Line shift (km/s)	Line width FWHM (km/s)	Intensity ( $10^{-16}\text{erg}$ $\text{s}^{-1}\text{cm}^{-2}$ )	Identification	$\lambda_{rest}$ ( $\mu\text{m}$ )
1469	1.0805	-400	4550	120	[S I] $3p^4\ ^3P\text{-}3p^4\ ^1D(1F)$	1.0820
1734	1.0805	-400	4550	350		
1822	1.0805	-400	4550	90		
2112	1.0805	-400	4550	25		
1469	1.0820	-550	5200	500	He I $2s^3S\text{-}2p^3P^o$	1.0830
1734	1.0820	-550	5200	95		
1822	1.0820	-550	5200	160		
2112	1.0820	-550	5200	75		
1469	1.0918	-800	4150	270	H I Pa $\gamma$	1.0938
1734	1.0918	-800	4700	35		
1822	1.0918	-800	4700	35		
2112	1.0922	-700	4700	35		
1469	1.1290	-400	4550	40	[S I] $3p^4\ ^3P\text{-}3p^4\ ^1D(1F)$	1.1306
1734	1.1290	-400	4550	110		
1822	1.1290	-400	4550	30		
2112	1.1290	-400	4550	8		
1469	1.1415	60	4650	300	Na I $3p^2P^o\text{-}4s^2S$ (3)	1.1397
1734	1.1415	-200	4650	130		
1822	1.1415	-200	4650	210		
2112	1.1415	-200	4650	115		
1469	1.2560	-450	4200	210	[Fe II] $a^6D_{9/2}\text{-}a^4D_{7/2}$	1.2567
1734	1.2555	-570	4050	145		
1822	1.2560	-450	4200	115		
2112	1.2560	-450	4200	75		
1469	1.2790	-800	4400	550	H I Pa $\beta$	1.2818
1734	1.2800	-800	4700	80		
1822	1.2790	-800	4700	75		
2112	1.2800	-700	4700	80		
1469	1.4410	-700	4650	620	[Fe I] $a^5D_4\text{-}a^5F_5$	1.4430
1734	1.4410	-700	4400	330		
1822	1.4410	-700	4650	200		
2112	1.4410	-700	4400	250		
1469	1.6051	-600	3400	100	[Si I] $3p^3P_1\text{-}3p^1D_2$ (0.01F)	1.6068
1734	1.6051	-600	3200	60		
1822	1.6051	-600	3000	60		
2112	1.6051	-600	3000	20		
1469	1.6437	-600	3400	280	[Si I] $3p^3P_2\text{-}3p^1D_2$ (0.01F)	1.6454
1734	1.6437	-600	3200	165		
1822	1.6437	-600	3000	165		
2112	1.6437	-600	3000	55		
1469	1.6426	-450	4200	150	[Fe II] $a^4F_{9/2}\text{-}a^4D_{7/2}$	1.6435
1734	1.6420	-550	4050	100		
1822	1.6426	-450	4200	85		
2112	1.6426	-450	4200	55		

NOTE: Uncertainties in Line shifts and Line widths are typically  $\pm 200$  km/s and  $\pm 500$  km/s respectively. The precision in the absolute intensities of the well-matched lines is about  $\pm 35\%$ , with higher accuracy for relative intensities within a single-band spectrum. However, where the matching is poorer the error in the line intensities is consequently larger. This tends to be an increasing problem at later epochs. To assess the precision of a line intensity given in the Table, the reader is advised to examine the quality of the model matches in the spectral plots (Figs. 2–5).

**Table 2** – *continued*

Epoch (days)	$\lambda_{peak}$ ( $\mu\text{m}$ )	Line shift (km/s)	Line width FWHM (km/s)	Intensity ( $10^{-16}\text{erg}$ $\text{s}^{-1}\text{cm}^{-2}$ )	Identification	$\lambda_{rest}$ ( $\mu\text{m}$ )
1469	1.9777	-700	4650	155	[Fe I] $a^5F_5-a^3F_4$	1.9804
1734	1.9777	-700	4400	110		
1822	1.9777	-700	4650	80		
2112	1.9777	-700	4400	25		
1469	2.0446	-450	4200	20	[Fe II] $a^4P_{5/2}-a^2P_{3/2}$	2.0457
1734	2.0437	-550	4050	15		
1822	2.0446	-450	4200	10		
2112	2.0446	-450	4200	6		
1469	2.0561	-550	5200	35	He I $2s^1S-2p^1P^o$	2.0580
1734	2.0561	-550	4900	35		
1822	2.0561	-550	5200	35		
2112	2.0561	-550	5200	8		
1469	2.1650	-450	4250	110	H I Br $\gamma$	2.1661
1734	2.1650	-450	4250	75		
1822	2.1650	-450	4250	35		
2112	2.1650	-450	4250	15		
1469	2.2095	60	4650	100	Na I $4s^2S-4p^2P^o$	2.2070
1734	2.2075	-200	4650	70		
1822	2.2075	-200	4650	50		
2112	2.2075	-200	4650	25		

NOTE: Uncertainties in Line shifts and Line widths are typically  $\pm 200$  km/s and  $\pm 500$  km/s respectively. The precision in the absolute intensities of the well-matched lines is about  $\pm 35\%$ , with higher accuracy for relative intensities within a single-band spectrum. However, where the matching is poorer the error in the line intensities is consequently larger. This tends to be an increasing problem at later epochs. To assess the precision of a line intensity given in the Table, the reader is advised to examine the quality of the model matches in the spectral plots (Figs. 2–5).

have also included narrow line profiles for the [Fe I] 1.443, 1.98  $\mu\text{m}$  (and the other lines of these multiplets). This line was not anticipated in the work of Lundqvist & Sonneborn (2001). However, the observed line profile shape on day 1533 in these wavelength regions led us to suspect that CSM [Fe I] emission may be making a small contribution to these features. At later epochs, the presence of [Fe I] emission from the CSM is much less convincing. Finally, we note the presence of an unidentified narrow feature at a wavelength of 1.485  $\mu\text{m}$  (after blueshifting by 289 km/s) on days 1533 and 1734.

## 4 DISCUSSION

### 4.1 The Physical Framework

The CSM spectra will be discussed elsewhere. Here we confine our discussion to the ejecta spectra. The framework for this section is based upon theoretical descriptions of the physical conditions in the ejecta and line strength predictions at very late times provided by Kozma & Fransson (1992), Fransson & Kozma (1993), Fransson, Houck & Kozma (1996) (FHK96), C97, dKLM98, and KF98a,b. While dKLM98 evolve their model to only 1200 days (*i.e.* 150 days prior to the beginning of our observations) their results are still relevant to the earlier part of the era considered here. KF98a follow the temperature and ionisation evolution

of their model to 2000 days, covering a significant portion of our era, but their line emission calculations (KF98b) stop at 1200 days. C97 consider the much later epoch of day 2875, which is near the end of our era.

During the era of the observations described here, the SN 1987A ejecta spectrum is produced in a rather exotic manner. The energy source of the nebula is the radioactive decay of a number of species created in the explosion (Woosley, Pinto & Hartmann 1989; Timmes et al. (1996)). These include  $^{56}\text{Co}$ ,  $^{57}\text{Co}$ ,  $^{60}\text{Co}$ ,  $^{44}\text{Ti}$  and  $^{22}\text{Na}$ . All emit  $\gamma$ -rays. In addition,  $^{56}\text{Co}$ ,  $^{44}\text{Ti}$  and  $^{22}\text{Na}$  emit energetic positrons and  $^{60}\text{Co}$  emits energetic electrons. By day 1348, the most significant energy sources were  $^{57}\text{Co}$  and  $^{44}\text{Ti}$ , contributing about one half and one quarter respectively of the deposited energy (Li, McCray & Sunyaev 1993; Timmes et al. 1996). Around day 1565, the dominant source of deposited energy became  $^{44}\text{Ti}$  and by about day 2000 more than half the deposited  $^{44}\text{Ti}$  energy was in the form of positrons. It is generally assumed that positrons are deposited “on the spot”. Consequently, given the  $\sim 60$  year lifetime of  $^{44}\text{Ti}$ , this means that once positron deposition is dominant, the rate of energy deposition approaches a constant value of  $1.3 \times 10^{36}$  erg/s per  $10^{-4} M_{\odot}$  of synthesised  $^{44}\text{Ti}$  (Woosley et al. 1989).

In order to reproduce the observed spectra and evolution of

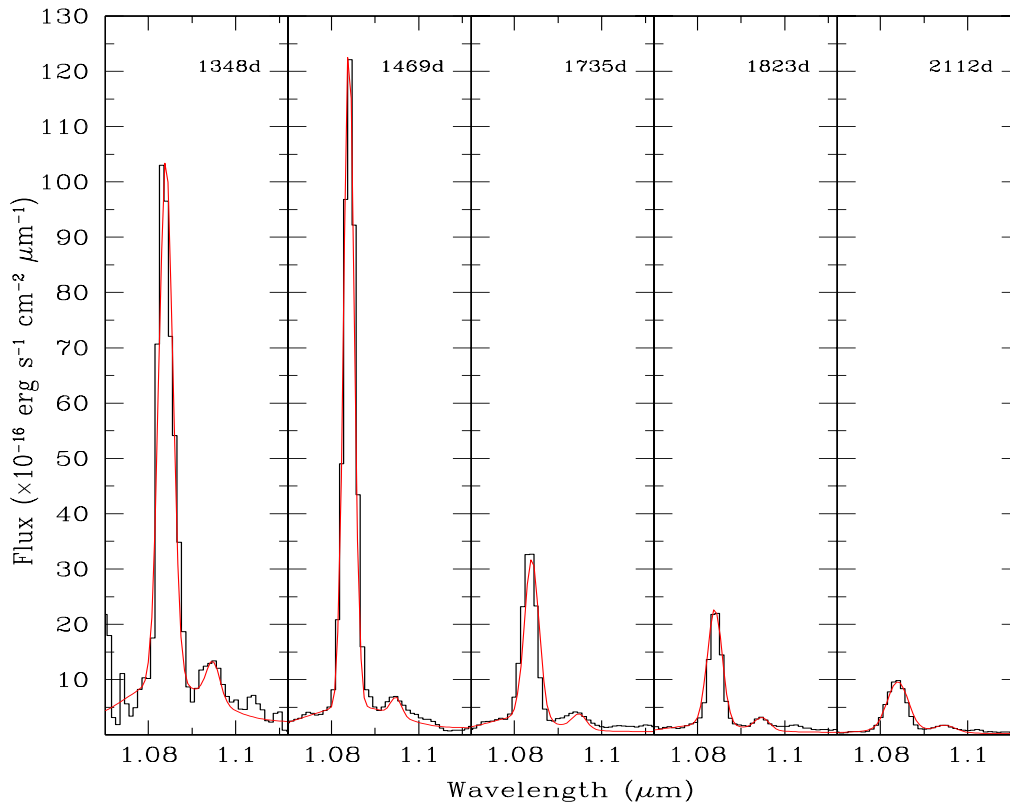


**Figure 7.** The evolution of the He I 1.083  $\mu\text{m}$  and Pa $\gamma$  CSM lines in the spectra of SN 1987A. The lines are always unresolved. Differences in the FWHM are due to variation in the seeing conditions. This is the reason for the increase in peak flux between days 1348 and 1469. However, the integrated intensities of the lines show a monotonic decline (see Table 3). The fluxing of the CSM spectra is better than  $\pm 40\%$ .

SN 1987A at late times, C97, dKLM98 and KF98a,b begin with model nebulae having a number of zones of differing chemical composition. These zones are arranged so as to reflect the strong, deep macroscopic mixing in SN 1987A for which there is a great deal of evidence (*e.g.* Arnett 1988, Pinto & Woosley 1988, Shigeyama, Nomoto & Hashimoto 1988, Woosley 1988, Haas et al. 1990, Spyromilio, Meikle & Allen 1990, Fassia & Meikle 1999). Light elements (H, He) are mixed down to low velocities, and iron group elements are mixed up to high velocities. C97, dKLM98 and KF98a,b introduce this mixing in different ways. However, they all invoke a macroscopically mixed “core” lying within  $\sim 2000$  km/s. (dKLM98 refer to the inwardly mixed H/He zones as the “inner envelope”.) The core thus contains zones that are H-rich, He-rich, intermediate-element-rich, and iron-group-rich, with the nebula being bathed in the radioactive decay energy. The core is generally of mass 4–6  $M_{\odot}$ . In addition, C97 and KF98a,b include an outer H-envelope of mass 10  $M_{\odot}$  extending out to a velocity of 6000–7000 km/s.

In general, the fraction of the radioactive decay energy that does not directly escape from the nebula is injected into the nebular material via Coulomb interaction with the positrons and Compton-scattered electrons. The energy of the resulting non-thermal high energy electrons then goes towards excitation, ionisation and heating of the nebula (KF98a). Three effects play important roles in the evolution of the

temperature and ionisation at the very late times considered here. These are the ionisation/thermal “freeze-out” effect, adiabatic cooling, and the “IR-catastrophe”. The first two are important in the H/He envelope, while the third plays an important role in the metal-rich core.

#### 4.1.1 Freeze-out

The ionisation freeze-out effect was suggested originally by Clayton et al. (1992) and by Fransson & Kozma (1993). These authors pointed out that as the SN evolves, there will eventually come a time when the recombination timescale exceeds the radioactive or expansion timescale, so that the rate of change in the level of ionisation slows significantly. Once this phase is reached, the bolometric luminosity exceeds that of the instantaneous radioactive decay deposition, since some of the luminosity results from recombination following ionisation at a significantly earlier epoch. In the model of KF98a,b the ionisation freeze-out phase begins at 800–900 days in most zones, but has a more pronounced effect on the luminosity in the H/He envelope. However, in their “inner-envelope” model, dKLM98 find that the freeze-out does not occur until much later than this. Instead, they identify a “thermal freeze-out” where the radiative cooling timescale exceeds that of the expansion timescale. In their model, this occurs before the ionisation freeze-out but, as with ionisation freeze-out, results in a luminosity exceeding that of the instantaneous radioactive decay deposition.

**Table 3.** Major CSM emission features observed on days 1469 to 2112

Epoch (days)	Intensity ( $10^{-16}$ erg $s^{-1} cm^{-2}$ )	Identification	$\lambda_{rest}$ ( $\mu m$ )
1469 1734	120(s) 135(s)	[S III]	0.9069
1469 1734	490(s) 265(s)	[S III]	0.9532
1348 1469 1734 1822 2112	3900 3600 1200 900 530	He I $2s^3S-2p^3P^o$	1.0830
1348 1469 1734 1822 2112	280 100 124 95 60	H I Pa $\gamma$	1.0938
1469 1734 1822 2112	60 45 30 20	[Fe II] $a^6D_{9/2}-a^4D_{7/2}$	1.2567
1348 1469 1734 1822 2112	340 100 90 70 65	H I Pa $\beta$	1.2818
1469 1734 1822 2112	90 40 30 15	[Fe II] $a^4F_{9/2}-a^4D_{7/2}$	1.6435
1469 1734 1822 2112	6 6 10 4	[Fe II] $a^4P_{5/2}-a^2P_{3/2}$	2.0459
1469 1734 1822 2112	70 35 30 20	He I $2s^1S-2p^1P^o$	2.0581
1469 1734 1822 2112	55 15 20 15	H I Br $\gamma$	2.1661

NOTE: The precision in the absolute intensities of the well-matched *IJ*-band lines is about  $\pm 35\%$ , with higher accuracy for relative intensities within a single-band spectrum. However, where the matching is poorer the error in the line intensities is consequently larger. This tends to be an increasing problem at later epochs. To assess the precision of a line intensity given in the Table, the reader is advised to examine the quality of the model matches in the spectral plots (Figs. 2–5). Vignetting problems in the *HK*-band CSM spectra (see text) means that the error in intensities is considerably larger than in the *IJ*-band (see text). (s) denotes that the fluxes were measured directly from the observations.

There is general agreement that by day 1200, the ejecta are predominantly neutral, but with a fraction of singly-ionised species resulting from the ionisation freeze-out and/or direct ionisation by non-thermal electrons. During 1350–2000 days the electron fraction is  $\sim 10^{-3}$  in the H-envelope, rising to 0.1 in the Fe-He zone (KF98a). At 3425 days, Lundqvist et al. (2001) calculate that the fraction of iron that is singly-ionised, is in the range 0.2–0.4.

#### 4.1.2 Adiabatic cooling

The adiabatic cooling becomes significant when the radiative cooling timescale becomes longer than the expansion timescale. For pure adiabatic cooling,  $T \propto t^{-2}$ . Owing to their lower density and metallicity, adiabatic cooling is already dominant as early as  $\sim 250$  days in the H-envelope and  $\sim 800$  days in the He-envelope (KF98a). For the H/He zones within the core, the higher densities mean that adiabatic cooling begins to dominate at 800–1000 days. While fine-structure line cooling (*cf.* IR catastrophe below) becomes the dominant radiative cooling mechanism in these zones, it never supersedes adiabatic cooling. Nevertheless, fine-structure line cooling may be significant in these regions (C97). KF98a find that the H-envelope temperature lies in the range 400–1000 K on day 1350, falling to a range of 150–300 K by day 2000. The temperatures of the H/He zones within the core fall from  $\sim 900$  K to  $\sim 300$  K over the same period. The day 2000 KF98a value compares well with the  $\sim 300$  K derived from the Balmer continuum by Wang et al. (1996) for about the same time. The model of C97 yields  $\sim 130$  K for the H-envelope at 2875 days, compared with  $350 \pm 100$  K derived from the Balmer continuum at that time.

#### 4.1.3 The IR catastrophe

Once the nebular heating/cooling rate drops below a certain level, cooling via low-lying fine-structure transitions dramatically overtakes optical and near-IR transitions as the dominant radiative cooling mechanism. Consequently the stabilising temperature falls abruptly from  $\sim 2000$  K to a few  $\times 100$  K, and the bulk of the nebula’s luminosity shifts to far-IR emission. This effect is known as the “IR Catastrophe”, and was predicted by Axelrod (1980) in his pioneering work on type Ia spectral models. Fransson & Chevalier (1989) predicted that it could also occur in core-collapse SNe such as SN 1987A. The first direct evidence for this phenomenon occurring in SN 1987A was obtained through the detailed study of the evolution of the near-IR/optical [Fe II] lines during the second year (Spyromilio & Graham 1992).

In the dense, metal-rich zones, fine-structure radiative cooling dominates for a considerable time. [Fe II]  $26 \mu m$  emission is particularly important. Fine-structure cooling is most pronounced in the Fe-rich zones (KF98a), where it commences at  $\sim 500$  days at 2700 K. According to KF98a, by the beginning of our observations (1348 days) the temperature in the Fe-He zone had fallen to  $\sim 150$  K, where it remained until 2000 days, after which adiabatic cooling became important. The IR catastrophe is also important for the intermediate mass element zones, where the temperature at

1350 days is 200–400 K, falling to 100–200 K by day 2000 (KF98). Both FK98b and dKLM98 find that, owing to the IR-catastrophe, [Fe II] 0.72, 1.26, 1.53, 1.64  $\mu\text{m}$  lines originating from the newly-synthesised iron in the core should have vanished by  $\sim 600$  days. However, detectable flux in these lines persists beyond this epoch. FK98b and dKLM98 attribute this to thermally-excited emission from primordial iron in the H-He envelope where the temperature remains above  $\sim 2000$  K until after day 1000. However, as indicated above, by 1350 days, the temperature in the H-He zone is below 1000 K and so thermally excited emission from these lines should be undetectable.

## 4.2 Near-IR ejecta lines at very late times

We can use the observed near-IR spectra to examine the physical scenario described above. The evolution of the intensities of the principal ejecta lines is illustrated in Figure 8.

### 4.2.1 Hydrogen Lines: $\text{Pa}\beta$ , $\text{Pa}\gamma$ , $\text{Br}\gamma$

The intensity and evolution of the H-lines in the adiabatic cooling phase is calculated by dKLM98 and KF98b up to 1200 days. For epochs  $> 2$  years, non-thermal ionisation from the ground state by Compton-scattered electrons dominates photoionisation from excited states (C97, KF98b). Non-thermal excitations are also important at epochs beyond 1000 days (KF98b). dKLM98 find that by day 800 the line ratios should be Case B. FK98b reach a similar conclusion, but with the transition to Case B in the core being a little later, at about 1000 days, being complete by day 1200. Thus, during our era, the H-spectrum is predicted to consist of a mixture of a low-temperature Case B H-recombination spectrum together with a contribution from direct non-thermal excitation (see KF98b for details). Line light curves are given by dKLM98 and KF98b for the near-IR lines  $\text{Pa}\alpha,\beta$ ,  $\text{Br}\alpha,\beta,\gamma,15$ . dKLM98 find that, for the well-observed near-IR H-lines  $\text{Pa}\beta$  and  $\text{Br}\gamma$ , their models makes satisfactory predictions to 1200 days. This is in spite of their non-inclusion of the envelope with its delayed recombination effects. The KF98b model light curve for  $\text{Br}\gamma$ , which includes delayed recombination effects in the envelope, is also in good agreement with the observations. Their model indicates that, by day 1200, the H-envelope is responsible for  $\sim 70\%$  of the  $\text{Br}\gamma$  flux, and that this fraction is growing. Both Fransson et al. (1996) and dKLM98 point out that derivation of total H-mass from the H-lines is difficult and subject to large uncertainties. Fransson et al. (1996) and KF98b make use of the line profiles in order to find the most appropriate model (and hence the mass of H). (In a sense, C97 also make use of the observed velocity distribution in determining the H-mass).

We examined the ejecta H-line fluxes to see if they yield the predicted low-temperature Case B ratios. These were first de-reddened assuming  $A_V = 0.6$  (Blanco et al. 1987). We find that the observed, de-reddened intensity ratio  $I_{\text{Pa}\gamma}/I_{\text{Pa}\beta} = 0.45 - 0.6$  for days 1469, 1734, 1822. Martin (1988) predicts a value of  $\sim 0.5$  for a temperature of 200–1000 K. Given the uncertainty in the relative line intensities, we judge that the observed ratios are consistent

with the predicted values. The uncertainties in the model matching are too large to make a useful judgement about the ratio on epoch day 2112. Martin (1988) also predicts  $I_{\text{Br}\gamma}/I_{\text{Pa}\beta} = 0.195$ . This is in fair agreement with the observed, de-reddened ratio of 0.18 on day 1469. Apparently poorer agreement is obtained on subsequent days. However, this is probably again due to model matching uncertainties, especially in the  $K$ -window. We conclude that, at least up to  $\sim 1800$  days, the observed H-spectra are consistent with the scenario of non-thermal ionisation/excitation within an environment dominated by adiabatic cooling.

### 4.2.2 Helium Lines: He I 1.083, 2.058 $\mu\text{m}$

As for hydrogen, theoretical considerations indicate that post-1000 day He-lines evolve in an environment where the temperature is dominated by adiabatic cooling, and the lines are driven by (a) non-thermal direct excitation, and (b) recombination following non-thermal ionisation. dKLM98 and KF98b point out that the 2.058  $\mu\text{m}$  line is uncontaminated by other ejecta species throughout the observations, and also find that it is optically thin in all regions after 700 days. Moreover, after  $\sim 700$  days, the 2.058  $\mu\text{m}$  line intensity is relatively insensitive to assumptions made about the He I 584  $\text{\AA}$  continuum destruction probability (KF98b). These considerations lead dKLM98 & KF98b to suggest that the post-600 day He I 2.058  $\mu\text{m}$  line can provide the best measure of the total helium mass. However, consideration of our spectra leads us to a more pessimistic view of the usefulness of the 2.058  $\mu\text{m}$  line in this situation. By day 1533, it was quite faint. To make matters worse it is blended with comparably-strong CSM flux in this line. Moreover, He I 2.058  $\mu\text{m}$  lies in a bad part of the atmospheric window. Consequently there is large uncertainty in the He I 2.058  $\mu\text{m}$  line flux. dKLM98 show that their model 2.058  $\mu\text{m}$  light curve provides a good match to the observations up to 1100 days. The KF98b light curve match is somewhat poorer, with a flux overproduction of about 40% between days 800 & 1100. The 2.058  $\mu\text{m}$  light curves of both dKLM98 and KF98b stop at 1200 days, but suggest a gradual slowing down. For the later epochs described here, to within the uncertainties, the observed fluxes fall on a plausible extrapolation of the dKLM98 model light curve, but continues to fall below that of the (extrapolated) KF98b light curve.

dKLM98 & KF98b agree that the He I 1.083  $\mu\text{m}$  line is more difficult to use for the determination of helium abundance. It is more temperature sensitive, and is optically thick for much longer than is the case for He I 2.058  $\mu\text{m}$ . Indeed, KF98b find the 1.083  $\mu\text{m}$  line to be optically thick in the He I region even beyond 2000 days. However, high optical depth in the inner zones may not be too important since, after 1200 days, the 1.083  $\mu\text{m}$  emission from the H-zone is predicted to dominate (and was already optically thin at 700 days). KF98b also point out that there may be contamination due to [S I] 1.082  $\mu\text{m}$ . Our empirical model matches also indicate that [S I] 1.082  $\mu\text{m}$  emission may be present. However, this line is part of a multiplet, with another component lying at 1.13  $\mu\text{m}$  and having about 0.3 of the intensity. Examination of this part of the spectrum (in spite of it being in a bad part of the atmospheric window) indicates that [S I] 1.082  $\mu\text{m}$  makes, at most, a relatively minor con-

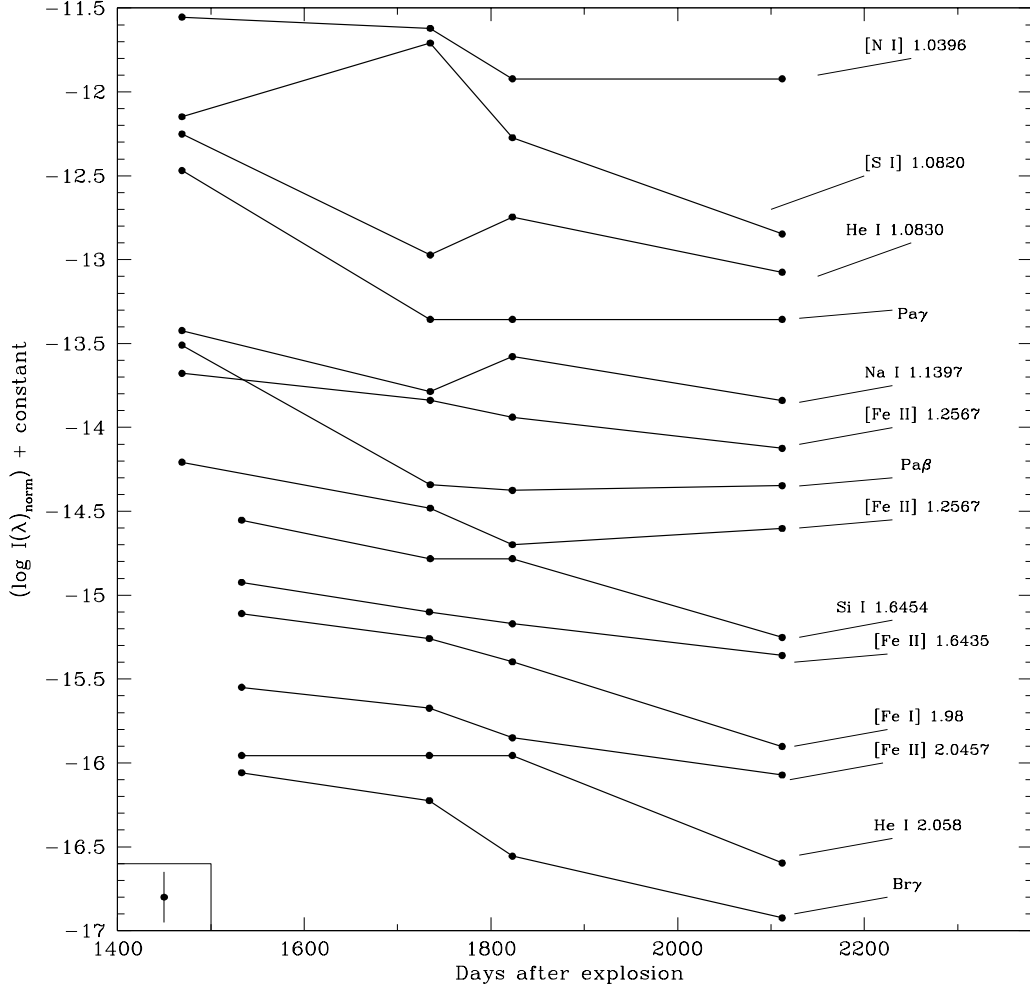


**Figure 8.** Evolution of the line intensities of the most prominent ejecta lines. The boxed point with the error bars indicates the typical  $\pm 35\%$  fluxing precision of the ejecta spectra. However, where the spectral model matching is poor, the error in intensity is consequently greater (see text).

tribution to the  $1.08 \mu\text{m}$  ejecta emission (see Fig. 3). We find that the observed fluxes of the He I  $1.083 \mu\text{m}$  line fall on plausible extrapolations of both the dKLM98 and KF98b model light curves.

#### 4.2.3 Forbidden lines of neutral species: [Si I], [S I] [Fe I]

The low temperature ( $T < 400 \text{ K}$ ) of the electron gas in the macroscopically-mixed core during the period of our observations implies that thermally-excited near-IR ejecta lines of [Si I], [S I] & [Fe I] should have faded below detectability. Yet, the [Si I] and [Fe I] lines are quite clearly present during this very late phase. (Strong blending makes the presence of the [S I] lines more ambiguous.) In particular, the [Si I]  $1.645 \mu\text{m}$  and [Fe I]  $1.443 \mu\text{m}$  lines are visible to beyond day 2000. The persistence of these lines provides valuable support for the proposition that, by this era, these lines are produced either by recombination or through direct excitation by non-thermal electrons.

The [Si I]  $1.6 \mu\text{m}$  multiplet is of particular interest here. FHK96 point out that for this species, recombination to the neutral state does not produce any significant line emis-

sion in the optical or near-IR region. Consequently, the [Si I]  $1.6 \mu\text{m}$  emission must be due entirely to direct excitation by non-thermal electrons. An interesting consequence of this is that the line luminosity will follow the instantaneous energy input, and will be independent of the ejecta temperature. At very late times this is dominated by the 100% absorption of  $^{44}\text{Ti}$  decay positrons. Thus, if the  $^{44}\text{Ti}$  scenario is correct, the luminosity in these lines should converge to a near-constant value. In Figure 8 we see that the [Si I]  $1.645 \mu\text{m}$  line fades by about a factor of 3 between days 1734/1822 and 2112. During this period, the radioactive energy deposition is dominated by  $^{44}\text{Ti}$  and would fade by a factor of about 1.5. Thus, to within the uncertainty in the line intensities, the evolution of [Si I]  $1.645 \mu\text{m}$  is consistent with the radioactive decay and energy deposition being dominated by  $^{44}\text{Ti}$  decay at these late times. We note that FHK96 also show that lines which are driven purely by non-thermal excitation, such as the [Si I]  $1.6 \mu\text{m}$  multiplet, have the potential to provide reliable, temperature-insensitive mass estimates, provided the line profile and the bolometric luminosity is also known.

C97 suggest that, by day 2875, virtually the entire positron



luminosity of the  $^{44}\text{Ti}$  is deposited in the Fe/Si-rich clumps. While cooling is mostly by ground-term fine-structure lines, about 10% ( $10^{35}$  erg/s) is via the UV-optical-NIR lines of neutral species. About 20% (of the  $10^{35}$  erg/s) is emitted as identified UV lines of Fe I and Si I with a further  $\sim 70\%$  being down-converted to numerous allowed and forbidden optical/NIR metal lines, forming a quasi-continuum. Of the remaining  $\sim 10^{34}$  erg/s, a substantial fraction flows into the [Si I] 1.6  $\mu\text{m}$  and [Fe I] 1.44  $\mu\text{m}$  near-IR multiplets. This appears to be supported by our low-resolution spectra (Figure 6) taken on days 2952 and 3158 where the [Fe I] 1.443  $\mu\text{m}$  and possibly the [Si I] 1.645  $\mu\text{m}$  features are still detected. The luminosity in just the [Fe I] 1.443  $\mu\text{m}$  line on day 2952 is about  $0.7 \times 10^{34}$  erg/s.

#### 4.2.4 Forbidden Lines of singly-ionised iron

As with the neutral forbidden lines, the low temperature of the ejecta during the era considered here means that there would have been negligible thermal excitation of the [Fe II] 1.26, 1.64  $\mu\text{m}$  multiplets. This includes the excitation of primordial iron in the H-envelope since, as mentioned above, even there it is expected that the temperature would be less than 1000 K by day 1350 (KF98a). This suggests, therefore, that the persistence of the [Fe II] lines must be due to recombination or direct excitation by non-thermal electrons. However, we note that C97 state that near-IR [Fe II] lines produced by radiative cascade are expected to be weak since the major radiative cascade to the ground level goes through optical forbidden lines and FIR lines of the ground term. Detailed modelling is required to test if this is in conflict with our detection of these lines.

### 4.3 Velocity behaviour in the ejecta lines

The FWHM velocities of the more prominent ejecta lines are listed in Table 2, Col. 4. The He I lines apparently exhibit the largest width, at  $\sim 5000$  km/s (FWHM). However, the uncertainty in this measurement is large due to strong blending of the He I ejecta lines with CSM lines and/or other species. The H I lines and the [Fe I], [Fe II] lines show widths of 4000–4500 km/s, while the [Si I] lines have widths closer to 3000 km/s. Even this latter value is higher than the  $\sim 2000$  km/s invoked for the macroscopically mixed core. Of particular interest is the fact that the [Fe I] and [Fe II] lines exhibit higher velocity widths than the [Si I] lines. We argued above that the persistence of the forbidden iron line emission during the era studied here must be driven by delayed recombination following freeze-out or through direct excitation by non-thermal electrons. Consequently, the high velocities in these lines imply that these processes must be occurring well out into the H/He envelope. Detailed modelling will be required to determine how much each process contributes to the line emission. If we favour the latter scenario, it immediately suggests that upward mixing was even greater than has been assumed hitherto. We note that velocities of at least  $\sim 3000$  km/s were observed in the [Fe II] lines as early as the end of year 1 (Paper I and Spyromilio et al. 1990, Haas *et al.* 1990). Moreover, Fassia & Meikle (1999) showed that the presence of the He I 1.083  $\mu\text{m}$  line on days 76–135 implied that upward mixing of  $^{56}\text{Ni}$  in the ejecta

of SN 1987A had extended to velocities as high as 3000–4000 km/s. Upward mixing of  $^{56}\text{Ni}$  to even higher velocities (over 5000 km/s) has been recently deduced by Mitchell et al. (2001) on the basis of the high strength of the Balmer lines a few days after explosion. Such high  $^{56}\text{Ni}$  velocities may be evidence of neutrino-instability-driven acceleration of radioactive nickel just after the core-bounce (*e.g.* Herant, Benz & Colgate 1992). Alternatively, these results may favour the jet-like explosion models of Nagataki (2000), in which the high velocity [Fe II] line profiles are well reproduced.

Another remarkable characteristic of these late-time spectra is the presence and persistence of blueshifts (with respect to the supernova rest frame) in the ejecta lines (Table 2, Col. 3), with values of typically  $-200$  km/s to  $-800$  km/s. Such shifts first appeared around day 600 (Paper II) and were attributed to the formation of dust, blocking out the red (far-side) wing of the line. With the persistence of the blueshifts to as late as day 2000 we conclude that very dense dust concentrations must have formed in the ejecta. However it is possible that asymmetry in the excitation conditions may also be contributing to the effect.

## 5 SUMMARY

We have presented near-IR spectra of SN 1987A covering the period 3.7 and 8.6 years post-explosion. This is the first time that IR spectra of a supernova has been obtained to such late epochs. We have described the measures taken to remove contamination from the nearby Stars 2 and 3. The resulting spectra comprise emission from both the ejecta and the bright circumstellar ring. The contributions from these two sources were separated out using an empirical spectral model. The CSM emission lines comprise recombination lines of H I and He I, and forbidden lines of [S III] and [Fe II]. The allowed ejecta spectra include lines of H I, He I, Na I, [Si I], [Fe I], [Fe II] and possibly [S I]. We are unable to confirm the presence of weak [Co I] and [Co II] lines as suggested by Bautista et al. (1995) on day 1445.

The intensity ratios and widths of the H I ejecta lines are consistent with the predicted low-temperature Case B recombination spectrum arising from non-thermal ionisation/excitation in an extended, adiabatically cooled H-envelope. Owing to difficulties with low signal-to-noise and CSM-ejecta blending, the He I 2.058  $\mu\text{m}$  ejecta line is probably of less value than pure ejecta theory would suggest.

Perhaps the most interesting result is the slow decline in the ejecta forbidden lines. This is particularly important for the [Si I] lines, since it supports the scenario that pure non-thermal excitation was taking place, driven increasingly predominantly by the decay of  $^{44}\text{Ti}$ . The data presented here offers the prospect of improved abundance measurements of silicon in the ejecta.

The FWHM of the ejecta lines provide evidence that the extensive mixing has occurred, with heavy elements reaching layers with velocities as high as  $\sim 3000$ – $4500$  km/s. The iron velocities were particularly high, and may provide sup-

port for the neutrino-instability fast-nickel scenario, or for a jet-like explosion. The blueshifts of the ejecta lines that had appeared around day 600 (Paper II) continued to be present. This probably indicates that dense concentrations of dust persisted in the ejecta even as late as day 2000. However, asymmetry in the excitation conditions may also contribute to the observed blueshifts.

The spectra presented here are unique. It is likely to be many years before such late-time near-IR observations are obtained for another supernova. Moreover, with the increasing interaction of the ejecta with the circumstellar ring, these near-IR spectra are probably the last from the “pristine ejecta” of SN 1987A that can be obtained.

## 6 ACKNOWLEDGEMENTS

We dedicate this paper to the memory of the late David Allen. He played a central role in the near-IR study of SN 1987A. He made particularly vital contributions to the work described here, both as project scientist for IRIS, and by carrying out most of the observations. He is sorely missed.

We thank Mike Burton, Stuart Lumsden, Raylee Stathakis and Chris Tinney for carrying out some of the observations, and the staff of the AAO for their support. We also thank Nick Suntzeff, Peter Challis and Peter Garnavich for the use of their unpublished data, and Emma Bowers, Robert Cumming and Gian Varani for assistance with the data reduction. This work is supported through PPARC Grant No. PPA/G/S/1997/00266.

## REFERENCES

- Allen D. A., Cragg T. A., 1983, *MNRAS*, 203, 777
- Allen D. A., Barton J. R., Burton M. G., Davies H., Farrell T., Gillingham P., Lankshear A., Lindner P., Mayfield D., Meadows V., Schafer G., Shortridge K., Spyromilio J., Straede J., Waller L., Whittard D., 1993, *PASAU*, 10, 298
- Arnett W. D., 1988, *ApJ*, 331, 337
- Axelrod T., 1980, PhD thesis, University of California
- Bailey J., Barton J. R., Conray P., Hillier D. J., Hyland A. R., Jones T. J., Shortridge K., Whittard D., 1988, *PASP*, 100, 1178
- Bautista M. A., Depoy D. L., Pradhan A. K., Elias J. H., Gregory B., Phillips M. M., Suntzeff N. B., 1995, *AJ*, 109, 729
- Blanco V. M., Gregory B., Hamuy M., Heathcote S. R., Phillips M. M., Suntzeff N. B., Terndrup D. M., Walker A. R., Williams R. E., Pastoriza M. G., Storch-Bergmann T., Matthews J., 1987, *ApJ*, 320, 589
- Chugai N., Chevalier R. A., Kirshner R. P., Challis P. M., 1997, *ApJ*, 483, 925 (C97)
- Crotts A. P., Heathcote S. R., 1991, *Nature*, 350, 683
- DeKool M., Li H., McCray R., 1998, *ApJ*, 503, 857 (dKLM98)
- Elias J. H., Frogel J. A., Matthews K., Neugebauer G., 1982, *AJ*, 87, 1029
- Elias J. H., Depoy D. L., Gregory B., Suntzeff, N. B., 1991, in “Supernova 1987A and other supernovae”, proceedings of an ESO/EIPC Workshop, eds Danziger I. J., Kj ar, p293
- Fassia A., 1999, PhD thesis, University of London
- Fassia A., Meikle W. P. S., 1999, *MNRAS*, 302, 314
- Fransson C., Houck J., Kozma C., 19996, in “Supernovae and supernova remnants”, Proceedings of the International Astronomical Union Colloquium 145, Cambridge University Press, eds McCray R., and Wang Z., p.211 (FHK96)
- Fransson C., Kozma C., 1993, *ApJ*, 408, 25
- Fransson C., Chevalier R. A., 1989, *ApJ*, 343, 323
- Haas M. R., Colgan S. W. J., Erickson E. F., Lord S. D., Burton M. G., Hollenbach D. J., 1990, *ApJ*, 360, 257
- Herant M., Benz W., Colgate S., 1992, *ApJ*, 395, 642.
- Jakobsen P., Jędrzejewski R., Macchetto F., Panagia N., 1994, *ApJ* 435, L47
- Kurucz R. L., 1993a, ATLAS9 Stellar Atmosphere Programs and 2 km s<sup>-1</sup> grid, (Kurucz CD-ROM No. 13)
- Kozma C., Fransson C., 1992, *ApJ*, 390, 602
- Kozma C., Fransson C., 1998a, *ApJ*, 496, 946 (KF98a)
- Kozma C., Fransson C., 1998b, *ApJ*, 497, 431 (KF98b)
- Li L., McCray R., Sunyaev R. A., 1993, *ApJ*, 419, 824
- Lundqvist, P., Sonneborn, G. 2001, in ASP Conf. Ser., SN 1987A: Ten Years After, ed. M. Phillips & N. Suntzeff (San Francisco: ASP), in press. (astro-ph/9707144)
- Lundqvist P., Kozma C., Sollerman J., Fransson C., 2001, *A&A*, 374, 629
- Martin P. G., 1988, *ApJS*, 66, 125
- Meikle W. P. S., Spyromilio J., Allen D. A., Varani G. -F., Cumming R. J., 1993, *MNRAS*, 261, 535 (Paper I)
- Meikle W. P. S., Allen D. A., Spyromilio J., Varani G. -F., 1989, *MNRAS*, 238, 193 (Paper II)
- Meikle W. P. S., 2001, in ASP Conf. Ser., SN 1987A: Ten Years After, ed. M. Phillips & N. Suntzeff (San Francisco: ASP), in press. (Available from <http://astro.ic.ac.uk/Research/stellar/supernovae/publications/>)
- Mitchell R. C., Baron E., Branch D., Lundqvist P., Blinnikov S., Hauschildt P. H., Pun S. J. C., *ApJ*, 556, 979
- Nagasaki S. 2000, *ApJS*, 127, 141
- Plait P. C., Lundqvist P., Chevalier R. A., Kirshner R. P., 1995, *ApJ*, 439, 730
- Pinto P. A., Woosley S. E., 1988, *Nat*, 333, 534
- Shigeyama T., Nomoto K., Hashimoto M., 1988, *A & A*, 196, 141
- Shortridge K., FIGARO General data reduction and Analysis Starlink MUD, RAL, June 1991
- Spyromilio J., Meikle W. P. S., Allen D. A., 1990, *MNRAS*, 242, 669
- Spyromilio J., Graham J. R., 1992, *MNRAS*, 255, 671
- Timmes F. X., Woosley S. E., Hartmann D. H., Hoffman R. D., 1996, *ApJ*, 464, 332
- Turner S. E., Suntzeff N. B., Elias J. H., Keane M., Phillips M. M., Depoy D., 1996, *BAAS* 189, 4505
- Walborn N. R., Phillips M. M., Walker A. R., Elias J. H., 1993, *PASP* 105, 1240
- Walker A. R., Suntzeff N. B., 1990, *PASP* 102, 131
- Wang Lifan, Wheeler J. C., Kirshner R. P., Challis P. M., Filippenko A. V., Fransson C., Panagia N., Phillips M. M., Suntzeff N., 1996, *ApJ*, 466, 998
- Weitzel L., Krabbe A., Kroker H., Thatte N., Tacconi-Garman L. E., Cameron M., Genzel R., 1996, *A&AS*, 119, 531
- Woosley S. E., Pinto P. A., Hartmann D., 1989, *ApJ*, 346, 395
- Woosley S. E., 1988, *ApJ*, 330, 218